Actinide (An = Th-Pu) Dimetallocenes: Promising Candidates for Metal-Metal Multiple Bonds

Cong-Zhi Wang[1], John K. Gibson[2], Jian-Hui Lan[1], Qun-Yan Wu[1], Yu-Liang Zhao[1], Jun Li[3], Zhi-Fang Chai[1,4], and Wei-Qun Shi*[1]

[1]Laboratory of Nuclear Energy Chemistry and Key Laboratory for Biomedical Effects of Nanomaterials and Nanosafety, Institute of High Energy Physics, Chinese Academy of Sciences, Beijing 100049, China

*E-mail: shiwq@ihep.ac.cn

[2]Chemical Sciences Division, Lawrence Berkeley National Laboratory, Berkeley, California 94720, United States

[3]Department of Chemistry and Key Laboratory of Organic Optoelectronics and Molecular Engineering of the Ministry of Education, Tsinghua University, Beijing 100084, China

[4]School for Radiological and interdisciplinary Sciences (RAD-X) and Collaborative Innovation Center of Radiation Medicine of Jiangsu Higher Education Institutions, Soochow University, Suzhou 215123, China

Supporting Information

Figure S1. Different views of the LUMO and LUMO+1 orbitals for Th_2Cp^*.

Figure S2-S6 The frontier MOs localized mainly on the An-An (An = Th-Pu) bonds

Figure S7-S11 NBO orbitals of the An-An bonds in the $An_2Cp^*_2$ complexes

Figure S12 Bond critical points for the $An_2Cp^*_2$ complexes

Table S1. Total energies after zero point energy corrections and the relative energies for the stable structures of An_2Cp^*

Table S2. Spin densities, spin contamination, bond distances for the $An_2Cp^*_2$ complexes calculated by the M06-L method

Table S3. Spin densities, spin contamination, bond distances, vibrational frequencies, Wiberg bond indices, and natural charges for An_2^{2+}

Table S4. Formal An-An bond order in $An_2Cp^*_2$ determined by the bonding molecular orbitals analysis

Table S5. Compositions of the An-An bonding in $An_2Cp^*_2$ obtained by natural bond orbital (NBO) analysis

Table S6. The changes in enthalpy and Gibbs free energy for dissociation reactions of $AnCp^*$ in the gas phase.

Table S7. The reaction energies for 2 ^8A $PuCp^*$ → ^{13}A $Pu_2Cp^*_2$ before and after inclusion of spin-orbit coupling effects.

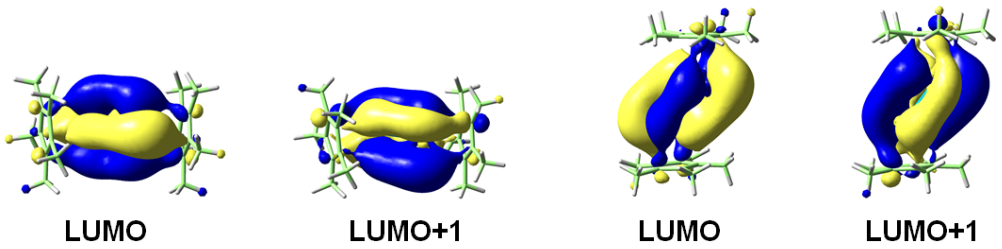

Figure S1. Different views of the LUMO and LUMO+1 orbitals for Th_2Cp^*.

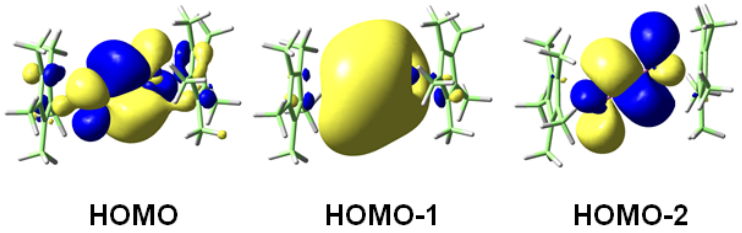

Figure S2. The frontier MOs localized mainly on the Th-Th bonds in the $Th_2Cp^*_2$ complex (HOMO, HOMO-1 and HOMO-2 are Th-Th bonding orbitals).

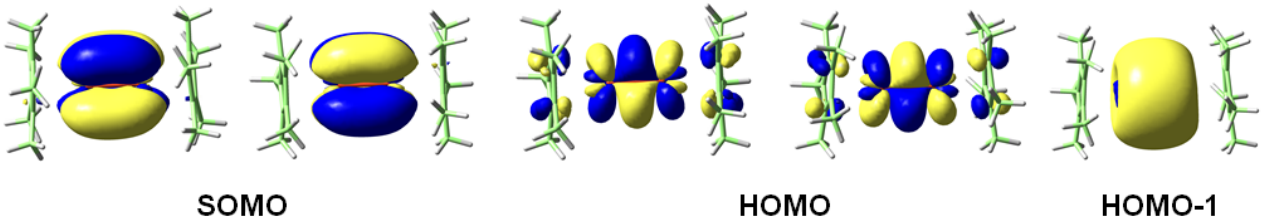

Figure S3. The frontier MOs localized mainly on the Pa-Pa bonds in the $Pa_2Cp^*_2$ complex (SOMO down to HOMO-1 are Pa-Pa bonding orbitals).

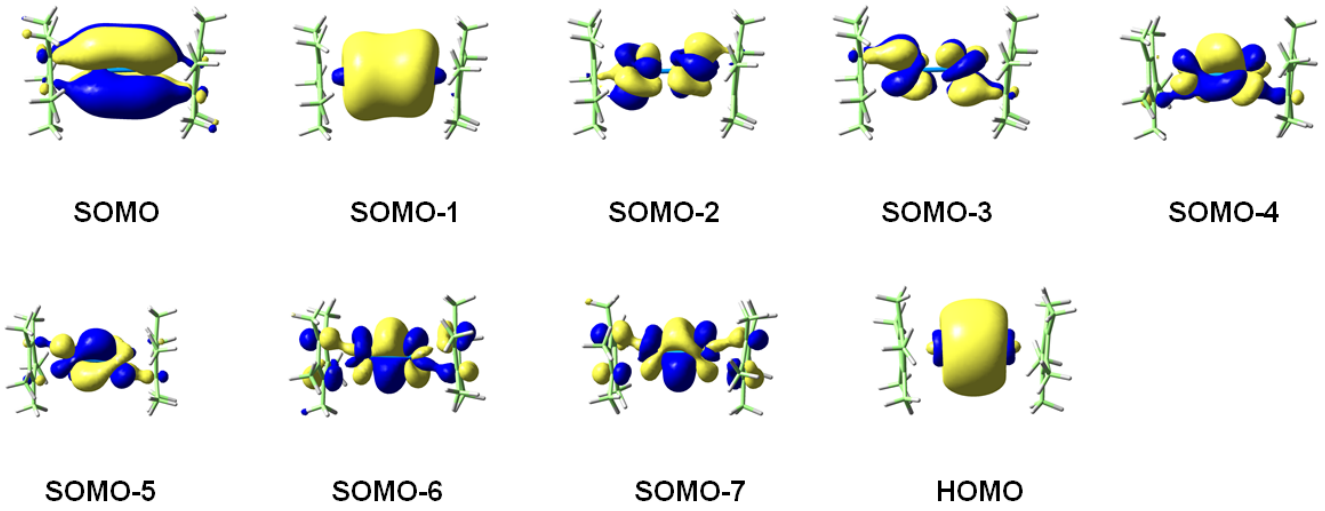

Figure S4. The frontier MOs localized mainly on the U-U bonds in the $U_2Cp^*_2$ complex (SOMO, SOMO-1, SOMO-4 down to HOMO are U-U bonding orbitals, and SOMO-2, SOMO-3 relating to the U-U antibonding orbitals).

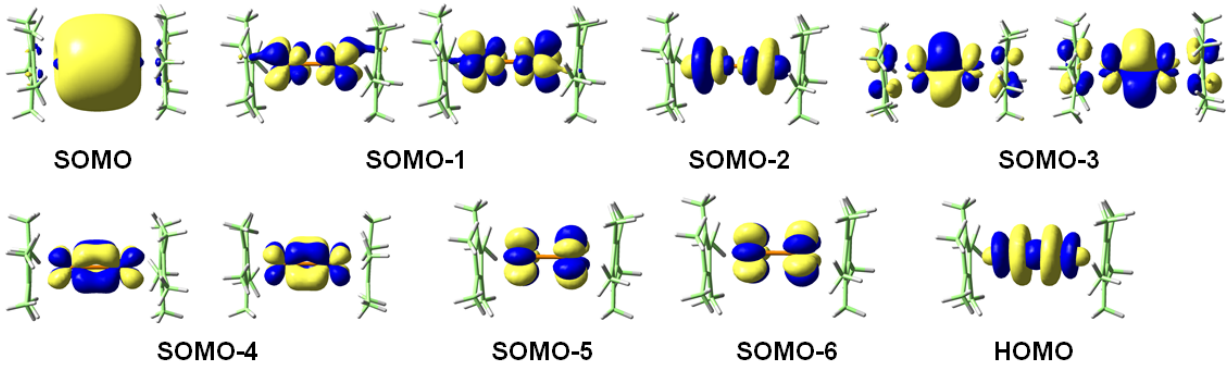

Figure S5. The frontier MOs localized mainly on the Np-Np bonds in the $Np_2Cp^*_2$ complex (SOMO, SOMO-3, SOMO-4, SOMO-6, HOMO are Np-Np bonding orbitals, and SOMO-1, SOMO-2, SOMO-5 relating to the Np-Np antibonding orbitals).

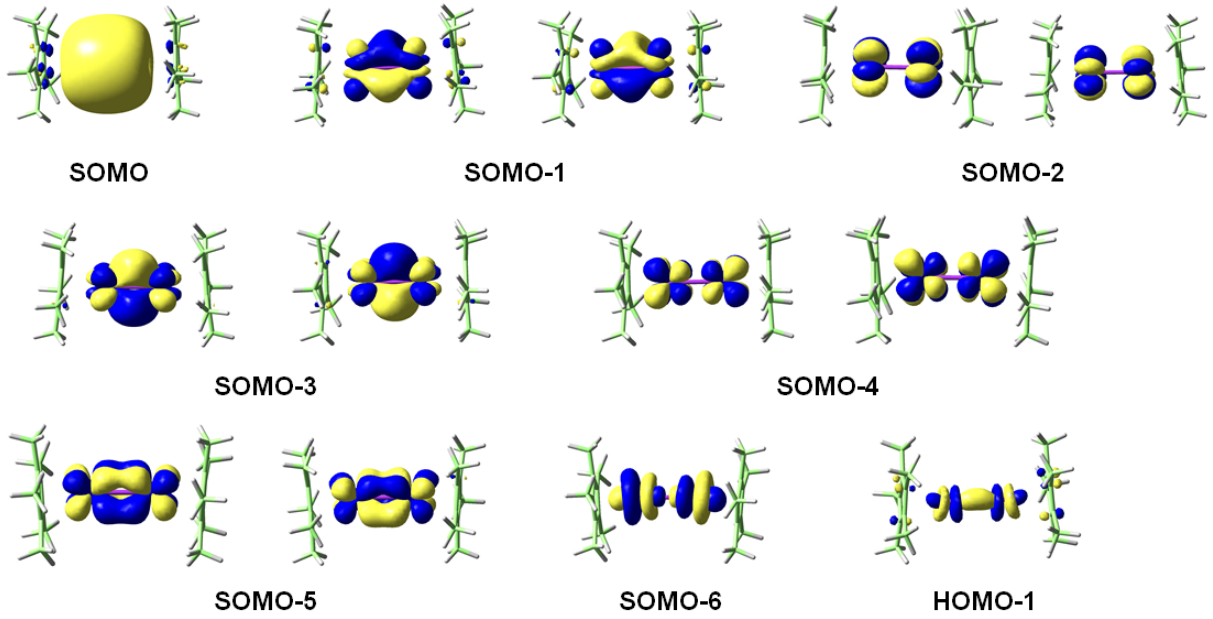

Figure S6. The frontier MOs localized mainly on the Pu-Pu bonds in the $Pu_2Cp^*_2$ complex (SOMO, SOMO-1, SOMO-3, SOMO-5, HOMO-1 are Pu-Pu bonding orbitals, and SOMO-2, SOMO-4, SOMO-6 relating to the Pu-Pu antibonding orbitals).

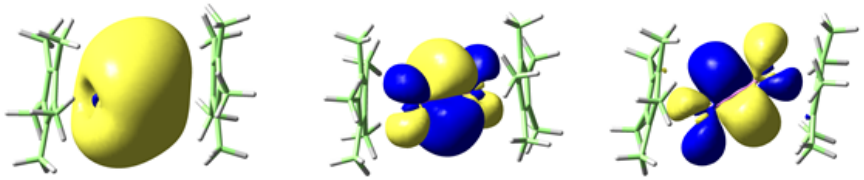

Figure S7. NBO orbitals of the Th-Th bonds in the $Th_2Cp^*_2$ complex.

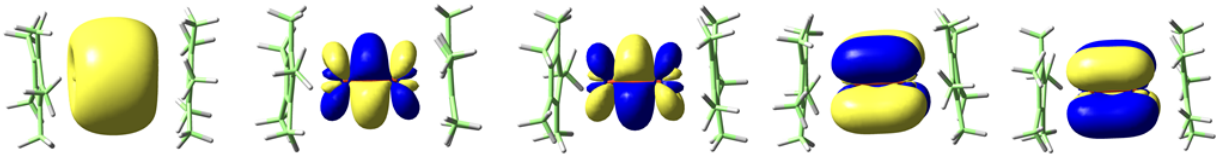

Figure S8. NBO orbitals of the Pa-Pa bonds in the $Pa_2Cp^*_2$ complex.

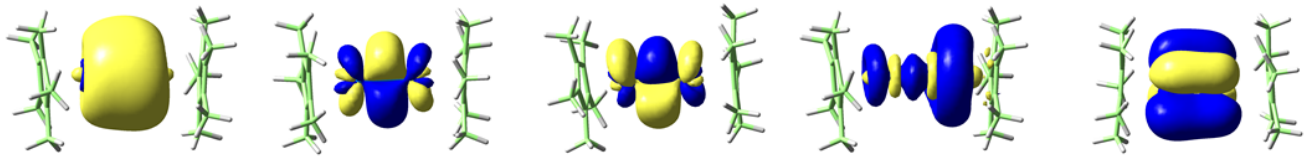

Figure S9. NBO orbitals of the U-U bonds in the $U_2Cp^*_2$ complex.

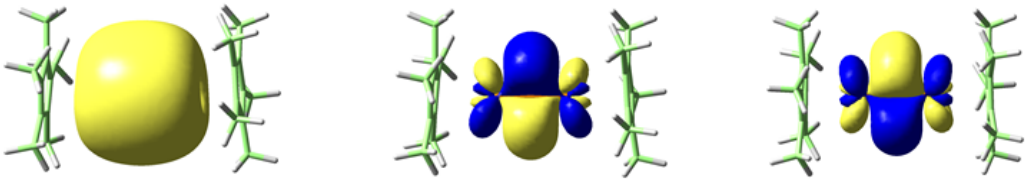

Figure S10. NBO orbitals of the Np-Np bonds in the $Np_2Cp^*_2$ complex.

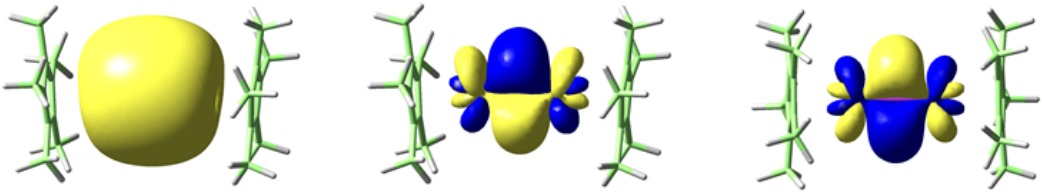

Figure S11. NBO orbitals of the Pu-Pu bonds in the $Pu_2Cp^*_2$ complex.

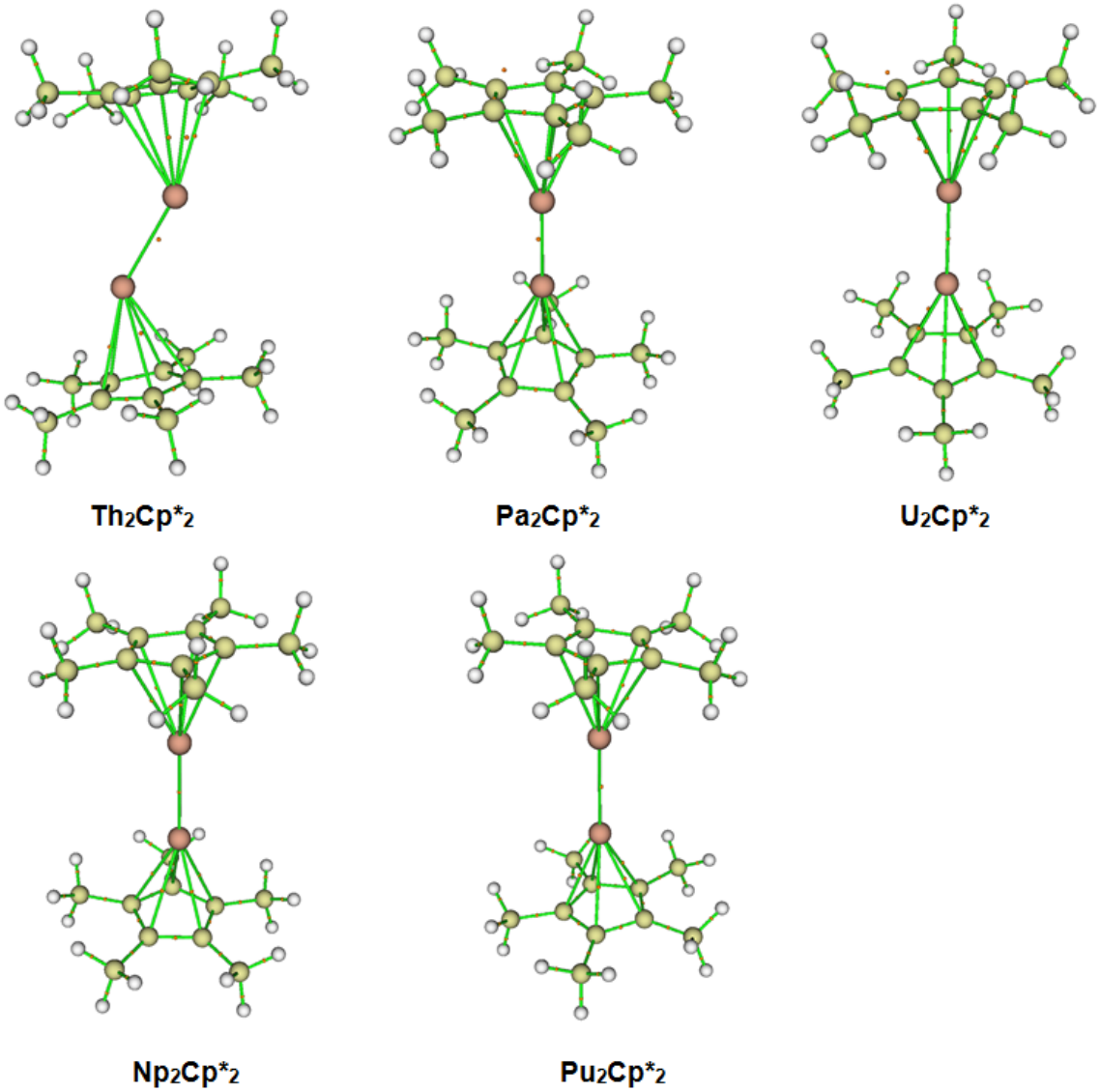

Figure S12. Bond critical points (BCPs, small orange spheres) for the $An_2Cp^*_2$ complexes. In all of the complexes the An-An BCP lies midway between the two actinide atoms.

Table S1. Total Energies after Zero Point Energy (ZPE) Corrections (E_{ZPE}, in Hartree) and the Relative Energies (ΔE_{ZPE}, in kcal/mol) for the Stable Structures of $An_2Cp^*_2$.

Species	States	E_{ZPE}	ΔE_{ZPE}
$Th_2Cp^*_2$	singlet	-1595.32677	0.0
	antiferromagnetic singlet	-1595.31149	9.6
	triplet	-1595.31086	10.0
	quintet	-1595.30767	12.0
	septet	-1595.28563	25.8
	nonet	-1595.17884	92.8
	11-et	-1595.07050	160.8
	13-et	-1594.94454	239.9
$Pa_2Cp^*_2$	singlet	-1662.74416	4.9
	antiferromagnetic singlet	-1662.69346	36.7
	triplet	-1662.75196	0.0
	quintet	-1662.73380	11.4
	septet	-1662.72962	14.0
	nonet	-1662.70557	29.1
	11-et	-1662.59633	97.7
	13-et	-1662.48752	165.9
$U_2Cp^*_2$	singlet	-1733.78371	27.6
	antiferromagnetic singlet	-1733.72286	65.8
	triplet	-1733.80631	13.4
	quintet	-1733.81796	6.1
	septet	-1733.82215	3.5
	nonet	-1733.82771	0.0
	11-et	-1733.81672	6.9
	13-et	-1733.70776	75.3
$Np_2Cp^*_2$	singlet	-1808.75750	83.8

	antiferromagnetic singlet	-1808.67721	134.2
	triplet	-1808.87203	12.0
	quintet	-1808.84234	30.6
	septet	-1808.85340	23.7
	nonet	-1808.86476	16.5
	11-et	-1808.89110	0.0
	13-et	-1808.86310	17.6
$Pu_2Cp^*_2$	singlet	-1887.64788	143.2
	antiferromagnetic singlet	-1887.87145	2.9
	triplet	-1887.85572	12.8
	quintet	-1887.81475	38.5
	septet	-1887.78366	58.0
	nonet	-1887.80147	46.8
	11-et	-1887.85316	14.4
	13-et	-1887.87608	0.0
	15-et	-1887.85368	14.1

Table S2. Spin Densities, Spin Contamination $\langle S^2 \rangle$, Bond Distances (Å) for the $An_2Cp^*_2$ Complexes Calculated by the M06-L Method.

Species	Symmetry	Spin State	$\langle S^2 \rangle$	Spin Density	Bond Lengths	
				An	An-An	An-C
$Th_2Cp^*_2$	C_1	singlet	0.00	—	2.834	2.790
$Pa_2Cp^*_2$	C_1	triplet	2.02	0.986, 1.010	2.367	2.772
$U_2Cp^*_2$	C_1	nonet	20.11	4.046, 4.032	2.581	2.684
$Np_2Cp^*_2$	C_1	11-et	30.05	5.103, 5.100	2.739	2.698
$Pu_2Cp^*_2$	C_1	13-et	42.18	6.045, 6.210	2.954	2.704

Table S3. Spin Densities, Spin Contamination $\langle S^2 \rangle$, Bond Distances (Å), Vibrational Frequencies (υ_{sym},

cm^{-1}), Wiberg Bond Indices (WBIs), and Natural Charges (Q) for An_2^{2+}.

Species	Spin State	$\langle S^2 \rangle$	Spin Density	Bond Lengths	υ_{sym}	WBIs	Q
			An	An-An	An-An	An-An	An
Th_2^{2+}	singlet	0.00	—	2.858	139	3.064	1.000
Pa_2^{2+}	triplet	2.06	0.997, 1.003	2.479	224	3.293	1.000
U_2^{2+}	nonet	20.07	4.000, 4.000	3.217	108	1.493	1.000
Np_2^{2+}	11-et	30.06	5.000, 5.000	3.206	101	1.494	1.000
Pu_2^{2+}	13-et	42.01	6.000, 6.000	4.088	53	1.004	1.000

Table S4. Formal An-An Bond Order in $An_2Cp^*_2$ Determined by the Bonding Molecular Orbitals Analysis.

Species	Bonding Electrons	Untibonding Electrons	An-An bond order (FBO)
$Th_2Cp^*_2$	6	0	3
$Pa_2Cp^*_2$	8	0	4
$U_2Cp^*_2$	8	2	3
$Np_2Cp^*_2$	8	4	2
$Pu_2Cp^*_2$	9	5	2

Table S5. Compositions of the An-An Bonding in $An_2Cp^*_2$ Obtained by Natural Bond Orbital (NBO)

Analysis.

Species	Bond Type	Element	Composition (%)	Contributions of Each Atomic Orbital (%)			
				5f	6p	6d	7s
$Th_2Cp^*_2$	σ	Th1	50.00	2.73	6.77	6.15	84.35
		Th2	50.00	2.73	6.77	6.15	84.35
	π	Th1	50.00	12.12	1.41	86.36	0.10
		Th2	50.00	12.12	1.41	86.36	0.10
	π	Th1	50.00	13.66	0.82	85.13	0.39
		Th2	50.00	13.66	0.82	85.13	0.39
$Pa_2Cp^*_2$	σ	Pa1	49.95	9.98	5.84	14.37	69.81
		Pa2	50.05	9.95	5.85	14.37	69.84
	π	Pa1	50.01	58.99	0.50	40.50	0.01
		Pa2	49.99	59.02	0.50	40.46	0.01
	π	Pa1	50.02	58.95	0.51	40.54	0.01
		Pa2	49.98	58.97	0.51	40.52	0.01
	δ	Pa1	50.30	17.22	0.01	82.77	0.00
		Pa2	49.70	18.17	0.01	81.82	0.00
	δ	Pa1	49.69	17.54	0.01	82.46	0.00
		Pa2	50.31	16.66	0.01	83.34	0.00
$U_2Cp^*_2$	σ	U1	53.39	25.82	4.03	11.87	58.28
		U2	46.61	31.81	2.89	15.74	49.56
	π	U1	41.39	59.78	1.03	39.15	0.03
		U2	58.61	66.90	1.26	31.82	0.02
	π	U1	41.63	57.28	1.31	38.04	3.36
		U2	58.37	62.48	1.24	32.66	3.62
	σ	U1	72.71	73.95	1.74	2.07	22.25
		U2	27.29	51.51	10.02	4.45	34.02
	δ	U1	43.75	29.14	0.09	70.72	0.05
		U2	56.25	15.11	0.01	84.83	0.05
$Np_2Cp^*_2$	σ	Np1	50.00	0.47	8.59	3.46	87.48
		Np2	50.00	0.47	8.59	3.46	87.48
	π	Np1	50.00	52.82	3.42	43.76	0.00
		Np2	50.00	52.82	3.42	43.76	0.00
	π	Np1	50.00	52.55	3.41	43.93	0.10
		Np2	50.00	52.55	3.41	43.93	0.10
$Pu_2Cp^*_2$	σ	Pu1	50.00	0.12	8.64	1.41	89.83
		Pu2	50.00	0.12	8.64	1.41	89.83

π	Pu1	49.92	66.56	2.33	31.11	0.00
	Pu2	50.08	66.67	2.32	31.01	0.00
π	Pu1	50.06	66.60	2.30	31.06	0.04
	Pu2	49.94	66.50	2.31	31.15	0.04

Table S6. The Changes in Enthalpy (ΔH_{298}) and Gibbs Free Energy (ΔG_{298}) (kcal/mol) for the Dissociation Reactions of $AnCp^*$ in the Gas Phase (298.15 K, 0.1 MPa).

Reactions	ΔH_{298}	ΔG_{298}
${}^2A$ $ThCp^* \rightarrow {}^2A_{1g}$ $Th^+ + {}^1A$ $[Cp^*]^-$	201.5	191.5
${}^3A$ $PaCp^* \rightarrow {}^3A_{1g}$ $Pa^+ + {}^1A$ $[Cp^*]^-$	185.4	176.3
${}^4A$ $UCp^* \rightarrow {}^4A_{1g}$ $U^+ + {}^1A$ $[Cp^*]^-$	184.5	174.5
${}^5A$ $NpCp^* \rightarrow {}^7A_{1g}$ $Np^+ + {}^1A$ $[Cp^*]^-$	172.9	184.5
${}^8A$ $PuCp^* \rightarrow {}^8A_{1g}$ $Pu^+ + {}^1A$ $[Cp^*]^-$	158.1	148.9

Table S7. The Reaction Energies (kcal/mol) for 2 ${}^8A$ $PuCp^* \rightarrow {}^{13}A$ $Pu_2Cp^*_2$ before and after Inclusion of Spin-Orbit Coupling (SOC) Effects. (The Scalar Relativistic (SR) and SOC Effects were Considered by the Zero-Order Regular Approximation (ZORA) Approach.)

Reaction	SR-ZORA	SO-ZORA
2 ${}^8A$ $PuCp^* \rightarrow {}^{13}A$ $Pu_2Cp^*_2$	-13.3	-14.3